J. Fluid Mech. (1989), *vol.* 205, *pp.* 453–467
Printed in Great Britain

Nonlinear progressive free waves in a circular basin

By PETER J. BRYANT
Mathematics Department, University of Canterbury, Christchurch, New Zealand

(Received 9 June 1987 and in revised form 20 January 1989)

A nonlinear analysis is presented of waves propagating around the free surface of water contained in a circular basin of finite uniform depth. The property that distinguishes these waves from unidirectional gravity waves is the occurrence of low-order resonant interactions between the components composing them. Steady waves in the neighbourhood of resonance are calculated in the fully nonlinear problem, when it is shown that multiple families of free-wave solutions, each family having a different set of resonating wave components, are associated with each of the water depths at which resonance occurs. Linear stability calculations indicate that most steady waves dominated by resonating wave components are linearly unstable. The nonlinear time evolution of perturbed waves is calculated as a check on the linear stability results, leading to doubts about the relevance of the linear prediction when marginal instability is said to occur.

1. Introduction

Resonant waves of large size can be generated by storms or earthquakes in enclosed regions such as harbours or bays. The resonance may result from external forcing of waves near their natural frequencies, or from internal forcing of some wave components by others. An example of the latter occurs in a circular basin near a depth to radius ratio of 0.831, when the first harmonic of a wave progressing around the basin forces resonantly the second harmonic of the wave, causing the two harmonics to be of comparable magnitude. A resonant triad is set up consisting of the first harmonic interacting with itself and the second harmonic. It is this internal forcing of wave components, in a free wave, which is investigated here. Both types of resonance may be present in externally forced waves, but only internal resonance can be present in free waves.

Weakly nonlinear methods for dynamical systems with a small number of degrees of freedom have been applied by Miles (1976, 1984*a*, *b*) to wave problems in fluid mechanics. He developed a Hamiltonian formulation for the analytical calculation of forced damped waves near resonance in closed basins, applying it in particular to circular basins. Prior assumptions had to be made about the ordering of the wave components, assumptions which may fail near internal resonance. The ordering then is influenced strongly by the relative strengths of the resonant interactions between the wave components. For this reason, it is desirable to use a fully nonlinear method at resonance without prior assumptions on the ordering of the wave components, particularly when damping is negligible. It will be shown that there are multiple wave solutions associated with the occurrence of internal resonance, with each family of steady wave solutions having a different ordering of the wave components. Miles (1984*a*) studied free-standing waves in a circular basin, but because progressive waves have fewer depth ratios at which internal resonance is significant than

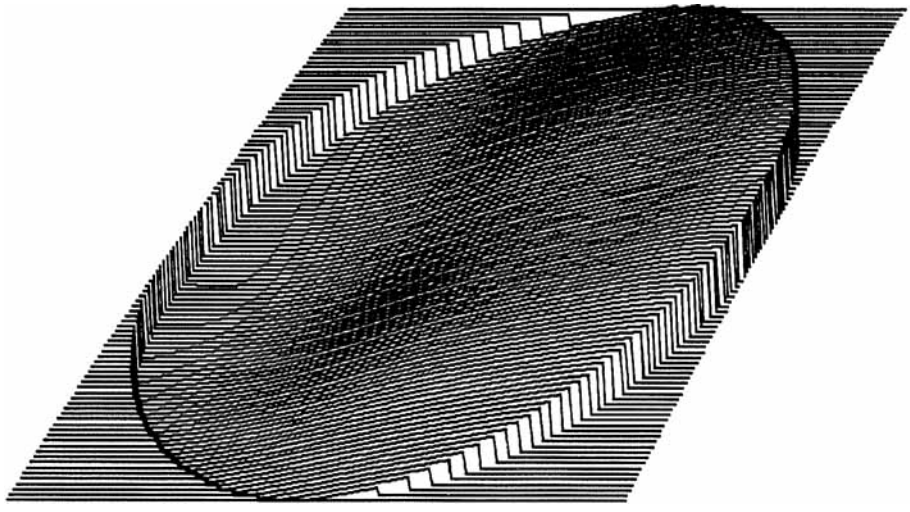

FIGURE 1. Steady circular progressive wave, $\epsilon = 0.02$, $d = 0.78$, drawn relative to the horizontal mean surface, without showing the sides of the circular basin. Vertical magnification 5.

standing waves have, the present investigation is confined to progressive waves. Preliminary calculations on standing waves showed good agreement with Miles' calculations only when the prior ordering assumptions are valid.

Wilton's ripples are another example of multiple families of steady waves subject to internal resonance, in this case capillary–gravity waves (Chen & Saffman 1979, 1980; Schwartz & Vanden-Broeck 1979). The usual ordering of Fourier coefficients in steady waves is to take the nth Fourier coefficient to be of nth order in the amplitude parameter (sometimes known as Stokes ordering). The multiple families of Wilton's ripples are calculated by reordering the Fourier coefficients. One family, for instance, has the first and second Fourier coefficients of the same order, and, like the example above, is associated with a resonant interaction between the first and second harmonics of the wave. Perturbation expansions with different orderings could be used to calculate the multiple families of steady wave solutions found here. The numerical method used instead finds all families of solutions because it makes no prior assumptions about the ordering of the wave components.

One example of a circular progressive wave is sketched in perspective in figure 1. The circular wave is drawn relative to the horizontal mean surface, without the sides of the circular cylinder being shown. In the notation defined in §2, it has a depth ratio $d = 0.78$, an amplitude ratio $\epsilon = 0.02$, and it is drawn with a vertical magnification of 5. The wave progresses in the θ-direction with an angular phase velocity $1.282(g/a)^{\frac{1}{2}}$. Like Stokes waves, the crest is further above the mean surface than the trough is below.

The water surface displacement $\eta(r, \theta, t)$ and the velocity potential $\phi(r, \theta, z, t)$ are both represented by truncated Fourier–Bessel series in the present method, with the coefficients in the series being chosen to fit Fourier–Bessel representations of the nonlinear free water-surface boundary conditions. This is an adaptation to a circular geometry of a fully nonlinear method developed previously for Cartesian geometries (Bryant 1985), and is based on the linear theory of waves in circular basins (Lamb 1945, §191). It is equivalent to collocation on a network of points in r and θ, and is a method of series truncation. One advantage it has over the usual collocation

methods is that the components of the series may be interpreted directly in terms of the linear wave components. Another advantage is that the residuals left by the boundary condition representations show directly which additional wave components need to be included to improve the numerical precision. The method is taken further than in previous applications, now including calculations of the linear stability of steady waves, and of the time evolution of unsteady waves.

The shallow-water approximation is widely applicable to wave propagation in enclosed regions, and finite difference schemes have been developed for the numerical solution of such models. However, the simplification or neglect of wave dispersion in the shallow-water approximation modifies severely the occurrence and contribution of wave resonance. It appears to be desirable to supplement wave calculations based on the shallow-water approximation with separate accurate calculations on the nature and contribution of resonant waves.

2. Progressive waves and resonance

A circular basin of radius a contains water of uniform depth, with d denoting the depth to radius ratio. Cylindrical polar coordinates r, θ, z are measured from an origin 0 at the centre of the mean horizontal free water surface, where the z-axis is vertically upwards, and r, z are non-dimensional multiples of a. The time variable t is a non-dimensional multiple of $(a/g)^{\frac{1}{2}}$. The water surface displacement, $\eta(r, \theta, t)$, and the velocity potential $\phi(r, \theta, z, t)$, are non-dimensional multiples of η_0 and $(ga)^{\frac{1}{2}}\eta_0$ respectively, where η_0 is the root-mean-square surface displacement (equation (2.6)). The amplitude ratio ϵ is defined to be η_0/a. The set of equations to be solved is

$$\phi_{rr}+\frac{1}{r}\phi_r+\frac{1}{r^2}\phi_{\theta\theta}+\phi_{zz}=0 \quad (r<1,\ -d<z<\epsilon\eta), \tag{2.1a}$$

$$\phi_r=0 \quad \text{on } r=1, \tag{2.1b}$$

$$\phi_z=0 \quad \text{on } z=-d, \tag{2.1c}$$

$$\eta_t-\phi_z+\epsilon\left(\eta_r\phi_r+\frac{1}{r^2}\eta_\theta\phi_\theta\right)=0 \quad \text{on } z=\epsilon\eta, \tag{2.1d}$$

$$\eta+\phi_t+\tfrac{1}{2}\epsilon\left(\phi_r^2+\frac{1}{r^2}\phi_\theta^2+\phi_z^2\right)=0 \quad \text{on } z=\epsilon\eta. \tag{2.1e}$$

Following the linear solution, waves progressing with non-dimensional angular velocity c in the positive θ-direction may be described by the Fourier–Bessel series

$$\eta=\sum_{m=0}^{\infty}\sum_{n=1}^{\infty}J_m(k_{mn}r)\,(a_{mn}\cos m(\theta-ct)+\alpha_{mn}\sin m(\theta-ct)), \tag{2.2a}$$

$$\phi=\sum_{m=0}^{\infty}\sum_{n=1}^{\infty}J_m(k_{mn}r)\frac{\cosh k_{mn}(z+d)}{\cosh k_{mn}d}(b_{mn}\sin m(\theta-ct)+\beta_{mn}\cos m(\theta-ct)), \tag{2.2b}$$

where

$$J'_m(k_{mn})=0 \quad (m=0,1,2,\ldots,n=1,2,\ldots). \tag{2.2c}$$

(k_{mn} is the nth zero of J'_m (Abramowitz & Stegun 1965, p. 411).) Equations (2.2) satisfy (2.1a, b, c) identically. The wave coefficients $a_{mn}, \alpha_{mn}, b_{mn}, \beta_{mn}$, all m, n, must be found so that they satisfy (2.1d, e) to any required numerical precision. Symmetric waves of steady shape are given with all coefficients a_{mn}, b_{mn} constant and α_{mn}, β_{mn} zero. The coefficients vary slowly with time in the linear stability and

m	n	d
2	2	0.831
3	2	0.279
3	3	0.455
3	4	0.748
4	2	0.158
4	3	0.249
4	4	0.330
4	5	0.423
4	6	0.542
4	7	0.721
4	8	1.204

TABLE 1. Depth ratios d satisfying the linear resonance relation (2.5)

time evolution calculations. The slow variation in time is interpreted in practical terms as meaning that the coefficients may be calculated accurately by Fourier analysis over each wave period, or equivalently, that their timescale is large compared with the wave period.

When the boundary conditions (2.1d, e) are linearized, and η, ϕ represented by only one (m, n) term of the series (2.2a, b), this term satisfies

$$a_{mn} = mcb_{mn}, \quad \alpha_{mn} = -mc\beta_{mn}, \tag{2.3a}$$

$$mc = (k_{mn} \tanh k_{mn} d)^{\frac{1}{2}}. \tag{2.3b}$$

For a nonlinear progressive wave dominated by the fundamental $(1, 1)$ wave component, (2.3b) provides a first approximation to the wave velocity,

$$c = (k_{11} \tanh k_{11} d)^{\frac{1}{2}}. \tag{2.4}$$

Resonance occurs for the nonlinear free wave near depth ratios at which (2.3b) is satisfied by this value of c, that is, near depth ratios d given by

$$m(k_{11} \tanh k_{11} d)^{\frac{1}{2}} = (k_{mn} \tanh k_{mn} d)^{\frac{1}{2}}. \tag{2.5}$$

All solutions of this equation up to $m = 4$ are listed in table 1. It should be emphasized that the values in table 1 provide only a first approximation to the depth ratios at which resonances occur. The nonlinear amplitude-dependent modification of (2.3), (2.4) is ignored, and it is assumed that it is the $(1, 1)$ wave component which is forcing all other wave components, one of them resonantly. It is noted that convergence to the linear theory, as ϵ tends to zero, is non-uniform at the depth ratios where internal resonance occurs.

The surface displacement η is a non-dimensional multiple of the root-mean-square surface displacement, or equivalently, η has a root-mean-square value of 1,

$$\frac{1}{\pi} \int_0^1 \int_0^{2\pi} \eta^2 r \, \mathrm{d}\theta \, \mathrm{d}r = 1, \tag{2.6}$$

from which

$$\sum_{n=1}^{\infty} \left(a_{0n}^2 J_0^2(k_{0n}) + \frac{1}{2} \sum_{m=1}^{\infty} (a_{mn}^2 + \alpha_{mn}^2) \left(1 - \frac{n^2}{k_{mn}^2}\right) J_m^2(k_{mn}) \right) = 1. \tag{2.7}$$

This normalization (suggested by Miles) makes constant ϵ equivalent to constant potential energy.

3. Methods of solution

Symmetric waves of steady shape are calculated by putting

$$a_{mn} = (a_{mn})_0, \quad b_{mn} = (b_{mn})_0, \quad \alpha_{mn} = 0, \quad \beta_{mn} = 0, \quad \text{all } m, n, \tag{3.1}$$

in (2.2a, b) and substituting in (2.1d, e). The latter equations are written, respectively,

$$F = \sum_{p=0} \sum_{q=1} F_{pq} J_p(k_{pq} r) \cos p(\theta - ct) = 0, \tag{3.2a}$$

$$G = \sum_{p=1} \sum_{q=1} G_{pq} J_p(k_{pq} r) \sin p(\theta - ct) = 0, \tag{3.2b}$$

from which

$$F_{pq}((a_{mn})_0, (b_{mn})_0, \epsilon, d, c) = 0, \tag{3.3a}$$

$$G_{pq}((a_{mn})_0, (b_{mn})_0, \epsilon, d, c) = 0, \tag{3.3b}$$

for all p, q. The number of functionals F_{pq}, G_{pq} is the same as the number of unknown amplitudes $(a_{mn})_0, (b_{mn})_0$. The normalization constraint (2.7) provides an additional equation, balancing the phase velocity c which is an additional unknown variable.

The numerical method of solution for symmetric steady waves is the same as that described previously (Bryant 1985). For given values of ϵ and d, a trial solution for the unknown variables $(a_{mn})_0, (b_{mn})_0$, and c is substituted into (2.1d, e) over a network of points in r and θ, and the functionals F_{pq}, G_{pq} calculated by inverting numerically the Fourier–Bessel series (using the trapezoidal rule for evaluating the inversion integrals). The derivatives of the functionals with respect to the unknown variables are calculated similarly by inverting the Fourier–Bessel series for the corresponding derivatives of (3.2). Newton's method is then used to improve the trial solution. The functionals F_{pq}, G_{pq} are found also for values of p and q outside those included in the calculation, in order to determine which wave modes should be added to the Fourier–Bessel series to improve the precision with which (2.1d, e) are satisfied over the complete range of r, θ, and t. Although the Fourier–Bessel series converge without difficulty at the moderate values of the amplitude parameter used here, Fourier series methods can be expected to fail at values of ϵ near breaking, when they are usually replaced by boundary integral techniques.

The linear stability of the symmetric waves is investigated by the Floquet method, by putting

$$a_{mn} = (a_{mn})_0 + \hat{a}_{mn}, \quad b_{mn} = (b_{mn})_0 + \hat{b}_{mn}, \quad \alpha_{mn} = \hat{\alpha}_{mn}, \quad \beta_{mn} = \hat{\beta}_{mn}, \quad \text{all } m, n, \tag{3.4}$$

in (2.2a, b), and substituting in (2.1d, e), with linearization in the time dependent perturbations $\hat{a}_{mn}, \hat{b}_{mn}, \hat{\alpha}_{mn}, \hat{\beta}_{mn}$. The Fourier–Bessel series are inverted numerically to produce a set of first-order linear differential equations for the perturbations. This set contains exactly twice the number of equations as that in the set of equations (3.3a, b). The set is solved by using the IMSL subroutine Eigrf, which finds the eigenvalues and eigenvectors of the stability matrix formed from the coefficients of the differential equations.

The time evolution of the unstable waves is calculated by letting the wave coefficients $a_{mn}, b_{mn}, \alpha_{mn}, \beta_{mn}$, all m, n, be slowly varying functions of time t. The Fourier–Bessel series are inverted numerically to yield a set of first-order nonlinear differential equations for the wave coefficients. The set is integrated step-by-step in time with the IMSL subroutine Dgear. The normalization constraint is evaluated at

each step as a check on the integration. It remains almost constant near value 1 for each perturbed wave until the effects of the truncation of the Fourier–Bessel series become significant.

4. Symmetric steady waves

Multiple families of steady waves are associated with the resonant depths listed in table 1. Steady waves arising from the major resonance between the fundamental (1, 1) wave component and the (2, 2) wave component near the depth ratio $d = 0.831$ are described here. The amplitude ratio ϵ is equal to 0.02 in all calculations. When this depth ratio is approached from larger values, the next significant resonance in table 1 occurs between the (1, 1) and (4, 8) wave components at a predicted value $d = 1.204$. The branching associated with this resonance actually occurs near $d = 1.4$ (when $\epsilon = 0.02$), the difference probably being due to nonlinear amplitude-dependent modification of the linear resonance relation (2.5) at the larger values of d where the tanh depth dependence is weak.

The wave coefficients a_{11}, a_{22}, a_{34} are plotted as functions of the depth ratio d in figures 2(*a*, *b*, *c*). The wave at the point A in the three figures, at depth ratio 1.2, has an ordering of the wave components consistent with non-resonant interactions between them, and is linearly stable. Moving along the curve, with d decreasing, a_{22} begins to increase suddenly at B, near $d = 0.85$. The normalization constraint (2.7) causes a_{11} to decrease correspondingly. Weakly nonlinear calculations (illustrated for example by Miles (1984*b*, figures 2 and 3)) show resonance curves with wave amplitudes increasing towards peaks, whose height is inversely related to the wave damping. Since the wave damping is assumed to be negligible here, the question of interest is the manner in which resonance is approached in a fully nonlinear model.

The rapid increase in a_{22} from B to C is consistent with weakly nonlinear calculations. The increase in a_{22} is reversed suddenly at C, as a_{34} increases suddenly in magnitude towards D. Although resonance between the (1, 1) and (3, 4) wave components is predicted in table 1 to occur near $d = 0.748$, the nonlinear modification of the linear resonance relation moves it here towards larger depth ratios. The rapid increase of a_{34} is itself reversed at D as both a_{47} and a_{48} increase in magnitude. However, these latter two coefficients are significant only for a limited range of d, to the point E, where a_{34} increases further in magnitude until it dominates the wave. At the end of the curve in the figure, at the point F, a_{11} is almost zero. A linear stability analysis shows that the wave is strongly unstable there. Linear stability calculations at different points along the curve found stable waves between A and B only, with the instability becoming stronger from B towards F.

The change in stability, according to the linear stability calculations, occurs near B with the appearance of marginally unstable wave modes. It is not known whether the instability is persistent in these marginal cases, or whether it is an artifice of the Floquet stability method. Equivalent calculations on resonating pendulums have found that the Floquet method does not determine accurately the point where stability changes. Stability for a given solution is found accurately only by longer time numerical integration of the evolution equations from initial conditions in the neighbourhood of the solution. It is believed that the difficulty arises here from linearization of the essentially nonlinear internal resonance phenomenon. For this reason, change of stability is not shown in figure 2, but it is believed to lie between B and C. This problem is discussed further in §5, example 2.

The computational method used in finding the curves is that outlined in §3,

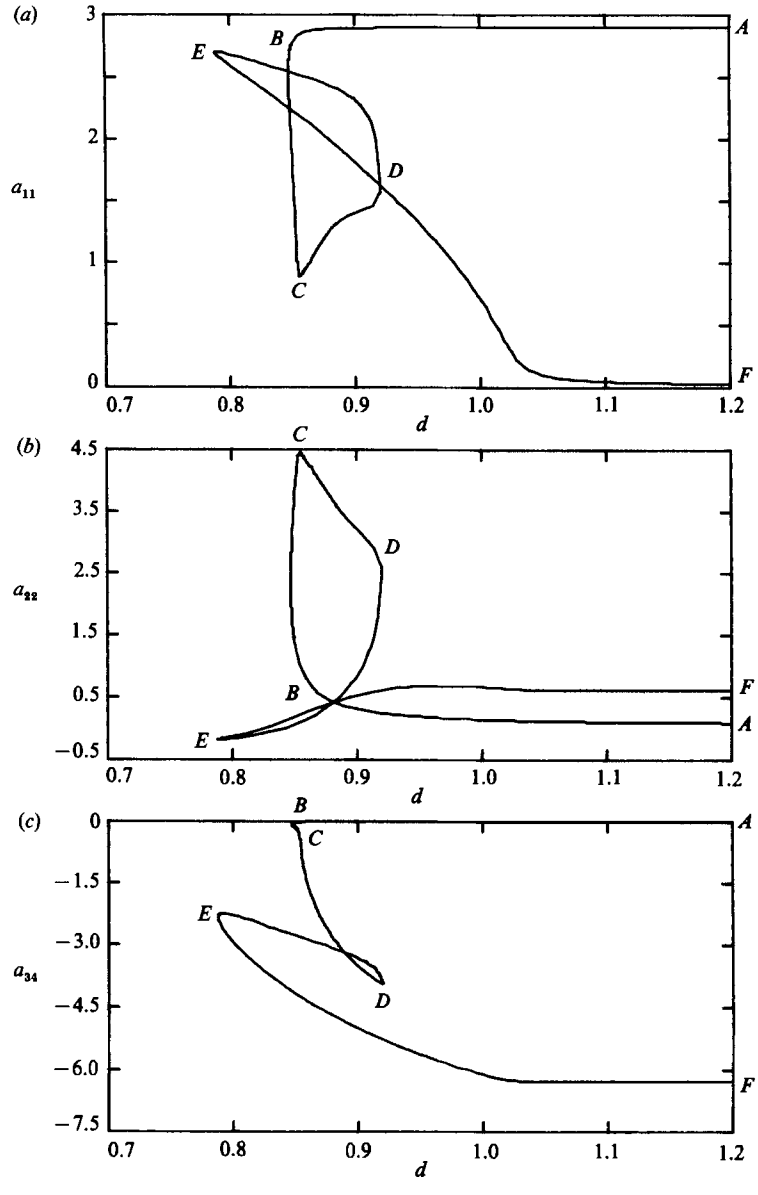

FIGURE 2. Dominant wave coefficients for steady waves as the (1, 1) *vs.* (2, 2) resonant depth ratio d is approached from larger values of d.

usually choosing d as the independent variable for stepping purposes. However, d was unsatisfactory for parts of the curves, where other variables were used for stepping from one wave solution to the next. Between B and C, for example, a_{22} was the independent variable for stepping purposes. For most calculations, the index m ran from 0 to 5 and the index n from 1 to 8 in (2.2a, b). Larger values of the indices were used only for particular examples in order to test the accuracy of the series expansions.

The Jacobian in Newton's method was calculated at each step and changes in sign of the determinant were investigated in more detail. Changes in sign occur at turning

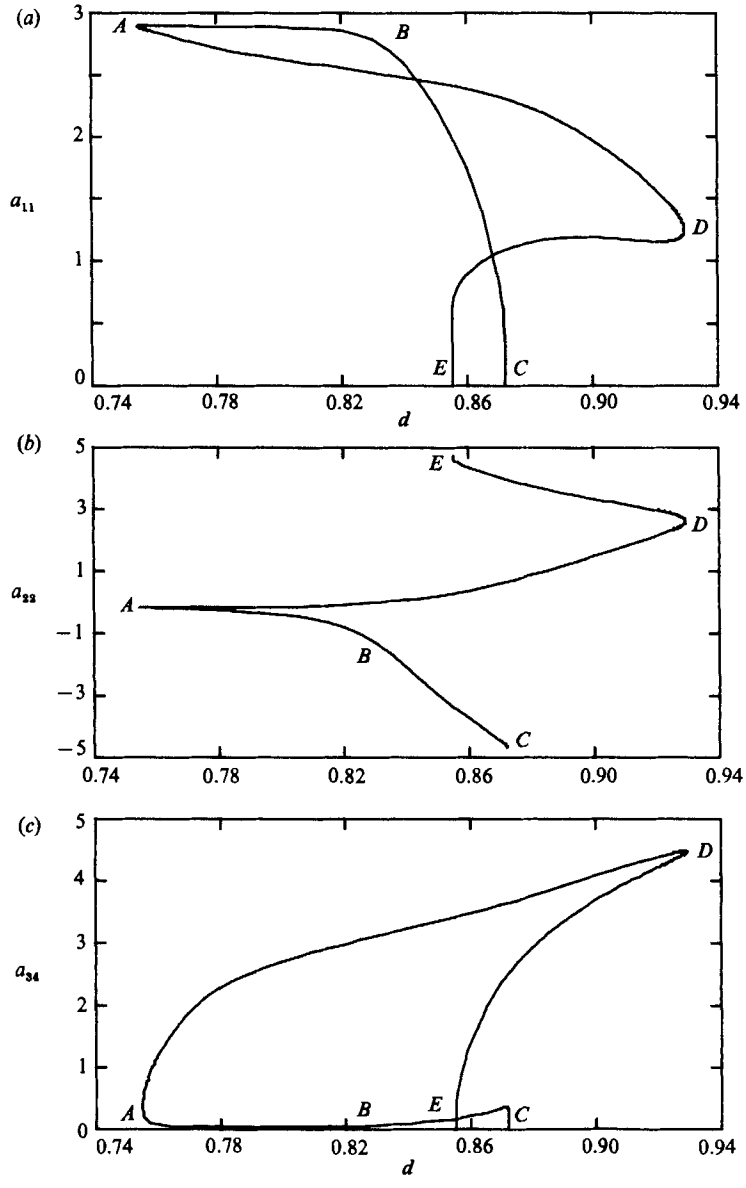

FIGURE 3. Dominant wave coefficients for steady waves in the neighbourhood of the (1, 1) *vs.* (2, 2) resonant depth ratio d.

points such as E in figure 2(*a–c*), and where the calculation jumps from one branch to another, from figure 2 into figure 3 for example. The behaviour of a_{22} *vs.* d in figure 2(*b*) is similar to that of A_M *vs.* κ in Chen & Saffman (1979, figure 8*b*), described there as limit-line behaviour. The pure wave on AB of figure 2(*b*) changes into a combination (1, 2) wave on BC, for which the first and second harmonics a_{11}, a_{22} are of comparable magnitude. The limit-line refers to the curve that BC approaches as a_{22} increases, this being the curve that extends back to a bifurcation point for pure waves near B. Figure 2(*a–c*) shows that the limit-line behaviour in the present fully nonlinear model is terminated at the point C by the occurrence of a second internal

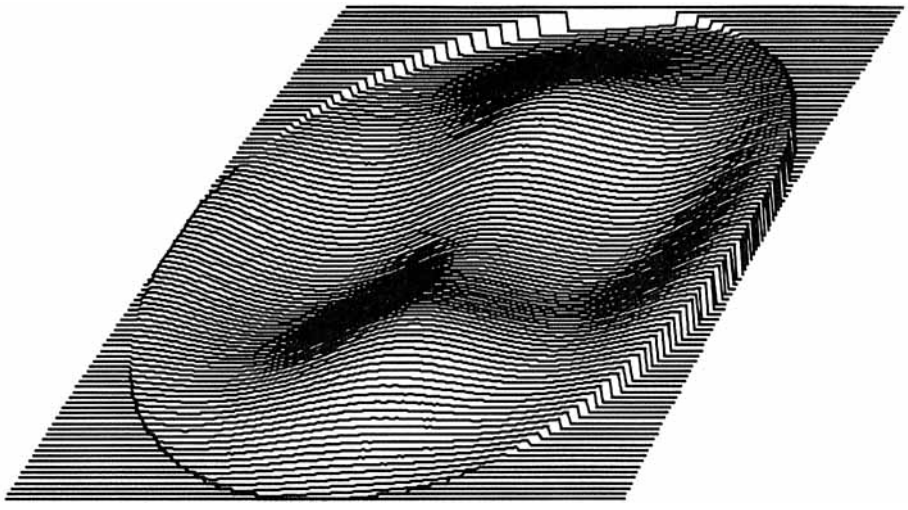

FIGURE 4. Steady circular progressive wave, $\epsilon = 0.02$, $d = 0.86$, drawn relative to the horizontal mean surface, without showing the sides of the circular basin. Vertical magnification 2.5.

resonant interaction, which in turn is followed by further internal resonant interactions at D and E. Chen & Saffman (1979, figure 8(*b*), shows oppositely-directed asymptotic behaviour for A_M on the two sides of the limit-line. The same phenomenon is found here, with a_{22} becoming large and negative as the limit-line is approached from smaller values of d.

The wave coefficients a_{11}, a_{22}, a_{34} of this second family of steady waves, on the other side of the limit-line, are plotted in figure 3(*a–c*). The section of these curves between A and B is the only part without significant resonant wave components, where the waves are found to be linearly stable. The a_{22} coefficient increases in magnitude from B to C as the depth ratio increases towards the predicted resonance for the $(1,1)$ and $(2,2)$ wave components. At the point C, all coefficients a_{mn}, m odd, are zero. These coefficients may be continued symmetrically to values of opposite sign on the other side of the axis in figure 3(*a, c*), because this is equivalent to a change in π of the origin in $\theta - ct$. No other wave components contibute resonantly from A to C.

If the steady wave curve is followed from A to D instead, a_{22} increases in magnitude towards resonance, with a_{34} increasing also. Resonance between the $(1,1)$ and $(3,4)$ wave components is predicted in table 1 to occur at a lesser depth ratio, but the nonlinear modification of the linear resonance relation causes it to be significant on this part of the curve. The a_{22} coefficient continues to increase from D to E, while a_{34} decreases to zero at E, as at C. The $(4,7)$ and $(4,8)$ wave components make a minor resonant contibution on the curve from A to E.

Figures 3*a*–3*c* are interesting for a number of reasons. They describe a family of steady wave solutions which exists only for a limited depth range, from $d = 0.755$ to $d = 0.930$. The family is dominated by the strong growth of the $(2,2)$ wave component due to resonant forcing by the $(1,1)$ wave component, which is predicted by the linear theory to occur near $d = 0.831$. There are two sections of curve side by side, from A to C and from A to E, on one of which a_{22} is the only significant resonant coefficient other than a_{11}, while on the other a_{22}, a_{34}, a_{47} and a_{48} all contribute resonantly. Even though the curve is cusped at A in figures 3(*a*) and 3(*b*), it changes smoothly at A with respect to a_{34} in figure 3(*c*).

The progressive steady wave at depth ratio $d = 0.86$ on the section BC of figure 3

is sketched in perspective in figure 4. In contrast with figure 1, (which lies on the section AB of figure 3), the $(2,2)$ wave component is significant, with more than twice the magnitude of the $(1,1)$ wave component, the two components being in resonant balance. The wave has four crests, on the wall at $\theta - ct = 0, \pi$, and at a smaller radius at $\theta - ct = \pm\frac{1}{2}\pi$. It is linearly unstable, but because the unstable growth rate is small, the perturbed wave is examined in more detail as example 2 in §5.

Further families of steady wave solutions have been calculated as this resonance is approached from lesser depth ratios. These families are influenced more strongly by the resonance between the $(1,1)$ and $(3,4)$ wave components near $d = 0.748$, and the $(1,1)$ and $(4,7)$ wave components near $d = 0.721$. (The latter is sketched in Bryant (1988, figure 1).) The common feature of these families is that, over most of the parameter range, a number of resonating wave components contribute significantly to the wave structure, and most of these waves are linearly unstable.

5. Linear stability and time evolution

The linear stability of steady progressive waves, symmetric in θ, is investigated with respect to small perturbations which may be non-symmetric in θ. The internal resonant interactions between wave components are nonlinear, which suggests that linearization may be valid for a limited time only. This limited validity occurs in the linear instability of Stokes waves to sideband modulation, reviewed for instance by Yuen & Lake (1982). The linearized calculation indicates instability, but the nonlinear resonant interaction between the two sideband wave components and the first and second harmonics of the Stokes wave stabilizes the wave. It is sufficiently stable in some cases that the initial modulated Stokes wave recurs cyclically during its time evolution. With this example as a precedent, it seems desirable to test both linearly stable and unstable perturbed waves, by making fully nonlinear calculations of their time evolution.

The linear stability is calculated by the Floquet method outlined in §3, using the non-symmetric progressive wave perturbation (3.4). Steady waves without significant resonant wave components are found to be linearly stable, while those with significant resonant wave components are linearly unstable. The characteristic equation for the eigenvalues λ of the stability matrix contains even powers of λ only, a property associated with the symmetry of the steady wave and with the time reversal invariance of non-dissipative systems.

The fully nonlinear time evolution of the perturbed waves is calculated by the method outlined in § 3, to compare the nonlinear evolution with that obtained from the linear stability calculations. Three examples are presented, first the stable wave sketched in figure 1, then the weakly unstable wave sketched in figure 4, and finally a more strongly unstable wave. The small initial asymmetric progressive wave perturbation

$$\hat{\eta} = 0.01 J_1(k_{11} r) \sin(\theta - ct), \tag{5.1}$$

is applied in each case, equivalent to

$$\alpha_{11} = 0.01, \quad \beta_{11} = -0.01/c, \quad \alpha_{mn} = \beta_{mn} = 0 \text{ otherwise}, \tag{5.2}$$

at time $t = 0$.

Example 1

$$\epsilon = 0.02, \quad d = 0.78, \quad c = 1.282.$$

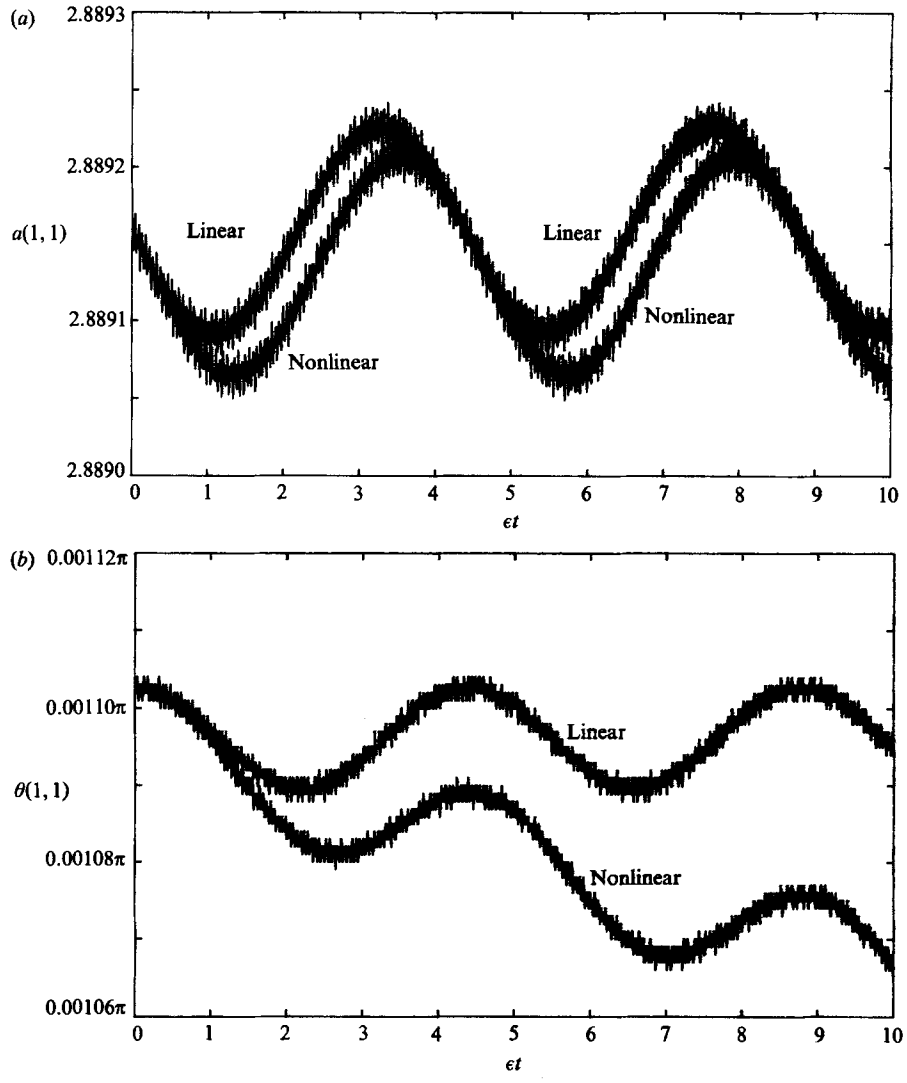

FIGURE 5. (*a*) The time evolution of the amplitude of the perturbed (1, 1) wave component, $\epsilon = 0.02$, $d = 0.78$, according to the linear and nonlinear calculations. (*b*) The time evolution of the phase of the perturbed (1, 1) wave component, $\epsilon = 0.02$, $d = 0.778$, according to the linear and nonlinear calculations.

The water surface displacement of the steady wave is

$$\eta = \sum_{m=0}^{5} \sum_{n=1}^{8} a_{mn} J_m(k_{mn} r) \cos m(\theta - ct), \tag{5.3}$$

where $a_{11} = 2.889, a_{22} = -0.271$ are the only wave coefficients exceeding 0.1 in magnitude. When the perturbation (5.1), (5.2) is applied, the linear stability solution satisfies

$$a_{11} = 2.889\,14 + 0.000\,07 \sin(1.433\epsilon t) + \ldots (10^{-5}), \tag{5.4a}$$

$$a_{11} = 2.009\,95 + 0.000\,06 \cos(1.443\epsilon t) + \ldots (10^{-5}). \tag{5.4b}$$

The amplitude $a(1, 1)$ and phase $\theta(1, 1)$, defined by

$$a(1, 1) = (a_{11}^2 + a_{11}^2)^{\frac{1}{2}}, \quad \theta(1, 1) = \tan^{-1}(\alpha_{11}/a_{11}),$$

are plotted in figure 5, from the linearized calculation and from the fully nonlinear calculation.

In comparing the linearized calculations with the fully nonlinear calculations in figure 5, it is noted that the two methods are independent, and that both sets were done on a supercomputer taking full advantage of its enhanced numerical precision. The linearized results are calculated by an algebraic eigenvalue method, in which the truncation of the Fourier–Bessel series make no significant contribution to the dominant eigenfrequencies and eigenmodes in figure 5. The nonlinear results are obtained from numerical integration of the evolution equations by a variable stepsize, predictor–corrector method, with the only significant numerical error arising from the gradual growth of the wave modes near truncation. The integrations were stopped when the mean potential energy (2.7) departed by more than 1% from its initial value (Unfortunately, the results from the supercomputer were stored to 6 decimal places only, so that subsequent analysis on a smaller computer to produce figure 5(*b*) gave the digitized appearance at the limit of storage accuracy of the phase.)

The dominant contribution to the perturbation of the (1, 1) wave component in both the linear and nonlinear solutions is from the eigenvector with the eigenvalue, $\lambda = \pm 1.433i$. There is good agreement between the amplitudes, $a(1,1)$, for the two solutions (figure 5*b*), but the phases, $\theta(1,1)$, differ in mean slope (figure 5*b*). This difference is equivalent to a small increase in the phase velocity of the perturbed wave in the nonlinear solution compared with the linear solution, and probably results from the small quadratic dependence of the phase velocity on the wave amplitude. It is clear from figure 5 that a small perturbation applied to the linearly stable wave leads to a small oscillation of the wave components in which internal resonance remains insignificant. However, if a larger nonlinear perturbation is applied, so that the perturbed wave lies near the branch AD in figure 3, rather than near the branch AB, internal resonance does become significant and the perturbed wave is unstable. This possibility is described in example 3.

Example 2

$$\epsilon = 0.02, \quad d = 0.86, \quad c = 1.301.$$

The water surface displacement of the steady wave is given by (5.3) with $a_{11} = 1.704, a_{22} = -3.756$ being the dominant wave coefficients. Linear stability calculations show that the perturbed (1, 1) coefficients satisfy

$$a_{11} = 1.7404 - 0.0074 \sin(0.196\epsilon t) + 0.0070 \sinh(0.0077\epsilon t) + \ldots (10^{-4}), \quad (5.5a)$$

$$\alpha_{11} = 0.0006 \cos(0.196\epsilon t) + 0.0106 \cosh(0.0077\epsilon t) + \ldots (10^{-4}). \quad (5.5b)$$

The amplitude $a(1,1)$ and phase $\theta(1,1)$ are plotted in figure 6, from both the linearized and nonlinear calculations.

This example lies on the section BC of figure 3, where the wave on AB has been changed by internal resonance to a combination (1, 2) wave for which the first and second harmonics have a comparable magnitude. The linearized calculations, (5.5*a*, *b*), predict weak instability, but this is an initial-value property only, without direct implications for the longer-time or asymptotic behaviour of the perturbed wave. Unfortunately, numerical integration of the fully nonlinear model had to be stopped at $\epsilon t = 10$ (about 80 wave periods) because of the increasing effect of series truncation. The linear and nonlinear calculations for the amplitudes in figure 6(*a*) show significant differences only towards the end of the integration. Repetition of the

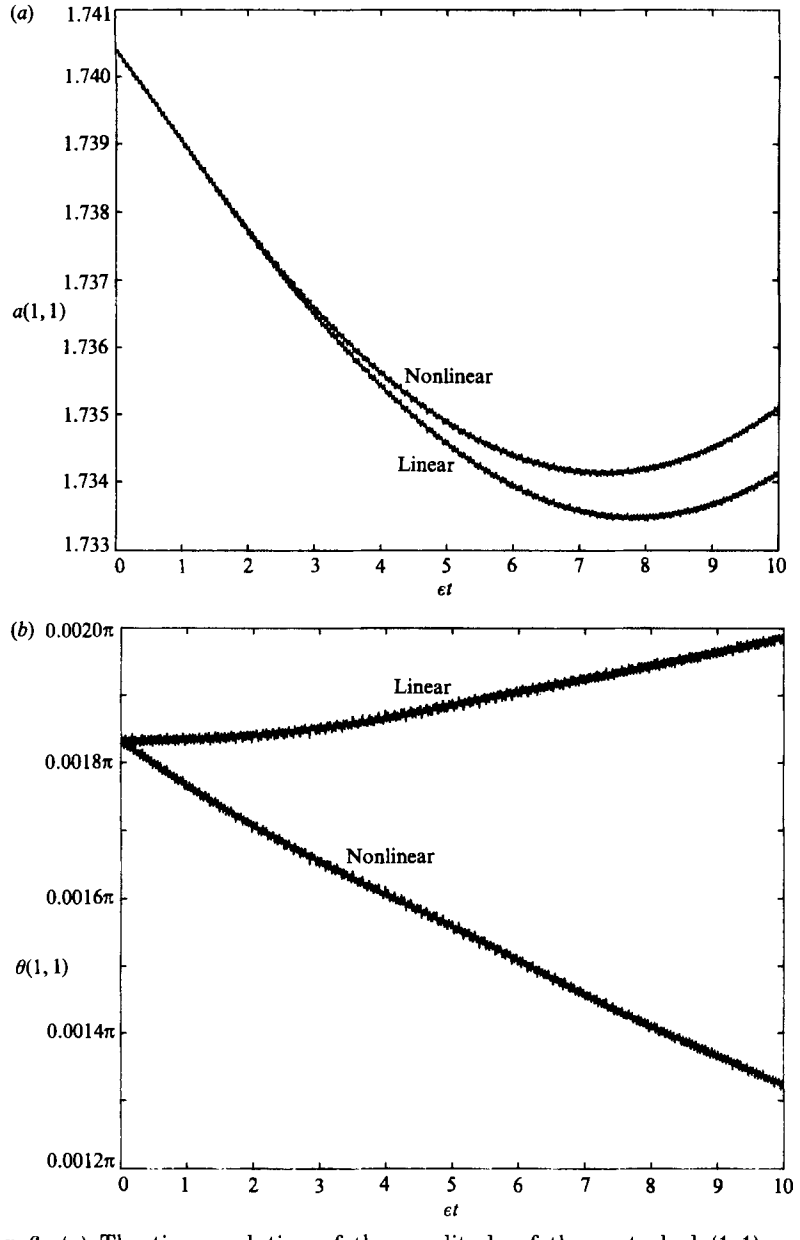

FIGURE 6. (*a*) The time evolution of the amplitude of the perturbed (1, 1) wave component, $\epsilon = 0.02$, $d = 0.86$, according to the linear and nonlinear calculations. (*b*) The time evolution of the phase of the perturbed (1, 1) wave component, $\epsilon = 0.02$, $d = 0.86$, according to the linear and nonlinear calculations.

numerical integration with more wave modes in the Fourier–Bessel series lengthens the time of validity of the nonlinear calculation beyond figure 6(*a*), at greater computing cost, but with a decreasing physical relevance because of the neglect of dissipation. If the numerical integration is made more realistic by including weak wavenumber-dependent linear damping, truncation effects are reduced or disappear because the high-wavenumber components are damped before they cause problems. The slopes of the mean phases in figure 6(*b*) differ for the linear and nonlinear

calculations probably because of the neglect in the linearized calculations of the quadratic dependence of phase velocity on amplitude.

Subsequent nonlinear calculations, at about the same wave amplitude and depth parameters as in this example, have been made on forced, weakly damped waves in a circular basin (Bryant 1988). The combination (1, 2) waves, with the first and second harmonics of comparable magnitude, are found to be stable over at least part of the range of the forcing amplitude and frequency for which internal resonance occurs. This result is of more relevance to waves in harbours or bays than is the longer-time behaviour of example 2 without dissipation.

Example 3

$$\epsilon = 0.02, \quad d = 0.78, \quad c = 1.283.$$

This steady progressive wave is on the section AD of the curves in figure 3, with the same depth ratio as example 1 (which is on the section AB). The values of a_{11} and a_{22} are close to those in the first example with $a_{11} = 2.714$ and $a_{22} = 0.194$, but now $a_{34} = 2.278$ is a significant wave coefficient. The stability matrix has a number of eigenvalues with non-zero real parts, the eigenvector with eigenvalue $\lambda = \pm 0.0098$ being dominant in the perturbation of the (1, 1) wave component, but that with eigenvalue $\lambda = \pm 1.2497$ being dominant in the perturbation of the (3, 4) wave component. Truncation errors become significant in the numerical integration of the fully nonlinear model at about $\epsilon t = 3$ (24 wave periods), even when more wave components are added, due to the unstable growth of the higher wavenumber components. Resonant interactions appear to play a role in transferring energy from the lower to the higher wavenumber components, causing the disintegration of the wave.

Example 3 has the same amplitude and depth ratios as example 1, but differs in the presence of a significant (3, 4) wave component in resonant balance with the (1, 1) wave component. Even though the linear stability analysis shows that example 1 is stable to small perturbations, the strength of the instability in example 3 suggests that example 1 is unstable to larger nonlinear perturbations containing a significant (3, 4) wave component. In other words, a wave which is stable to small perturbations may exhibit unstable growth in the presence of larger externally generated perturbations containing a significant higher wavenumber component internally resonant with the given wave. This form of unstable wave growth is thought to occur in a particular harbour on the rare occasions when ocean swell of the appropriate spectral content and direction is able to propagate directly in the harbour entrance, causing resonant amplification of otherwise small waves within a partially enclosed region of the harbour.

6. Discussion

The main result emerging from this investigation is the importance of internal resonance for free waves in enclosed regions. The weakly nonlinear analysis of Miles (1976, 1984*a*, *b*) describes all the essential features of the approach to resonance. However, the prior ordering of the wave components, which is made in a weakly nonlinear theory, prevents the calculation of waves with different orderings of the wave components, such as are caused by internal resonances. Fully nonlinear calculations, without prior ordering assumptions, reveal an abundance of free progressive waves with resonant wave components. Families of waves with different

sets of resonant wave components are associated with each of the depth ratios listed in table 1. It is expected that if higher numerical precision were used, further families could be found associated with depth ratios at which higher resonances occur.

Weak dissipation significantly modifies the internal resonant interactions with the higher-wavenumber components. For this reason, dissipation plays a stabilizing role for waves in enclosed regions subject to internal resonance. Calculations on such waves should include dissipative effects, particularly calculations over longer times.

Most of this investigation was done during a period of leave at the Institute for Geophysics and Planetary Physics, University of California, San Diego. I am grateful to John W. Miles for making this visit possible, and for discussions on the calculations. Acknowledgement is made to the San Diego Supercomputer Center, which is sponsored by the National Science Foundation, for the computing time used in this research.

REFERENCES

ABRAMOWITZ, M. & STEGUN, I. A. 1965 *Handbook of Mathematical Functions*. Dover.

BRYANT, P. J. 1985 Doubly periodic progressive permanent waves in deep water. *J. Fluid Mech.* **161**, 27–42.

BRYANT, P. J. 1988 Nonlinear waves in circular basins. *Nonlinear Water Waves* (ed. K. Horikawa & H. Maruo). Springer-Verlag.

CHEN, B. & SAFFMAN, P. G. 1979 Steady gravity-capillary waves on deep water. I. Weakly nonlinear waves. *Stud. Appl. Maths* **60**, 183–210.

CHEN, B. & SAFFMAN, P. G. 1980 Steady gravity-capillary waves on deep water. II. Numerical results for finite amplitude. *Stud. Appl. Maths* **62**, 95–111.

LAMB, H. 1945 *Hydrodynamics*. Dover.

MILES, J. W. 1976 Nonlinear surfaces waves in closed basins. *J. Fluid Mech.* **75**, 419–448.

MILES, J. W. 1984*a* Internally resonant surface waves in a circular cylinder. *J. Fluid Mech.* **149**, 1–14.

MILES, J. W. 1984*b* Resonantly forced surface waves in a circular cylinder. *J. Fluid Mech.* **149**, 15–31.

SCHWARTZ, L. W. & VANDEN-BROECK, J.-M. 1979 Numerical solution of the exact equations for capillary-gravity waves. *J. Fluid Mech.* **95**, 119–139.

YUEN, H. C. & LAKE, B. M. 1982 Nonlinear dynamics of deep-water gravity waves. *Adv. Appl. Mech.* **22**, 67–229.